

# Wrinkling and folding patterns in a confined ferrofluid droplet with an elastic interface

Pedro H. A. Anjos,<sup>1,\*</sup> Gabriel D. Carvalho,<sup>2,†</sup> Sérgio A. Lira,<sup>3,‡</sup> and José A. Miranda<sup>1,§</sup>

<sup>1</sup>*Departamento de Física, Universidade Federal de Pernambuco, Recife, Pernambuco 50670-901, Brazil*

<sup>2</sup>*Centro Brasileiro de Pesquisas Físicas, Rio de Janeiro, Rio de Janeiro 22290-180, Brazil*

<sup>3</sup>*Instituto de Física, Universidade Federal de Alagoas, Maceió, Alagoas 57072-900, Brazil*



(Received 3 December 2018; published 19 February 2019)

A thin elastic membrane lying on a fluid substrate deviates from its flat geometry on lateral compression. The compressed membrane folds and wrinkles into many distinct morphologies. We study a magnetoelastic variant of such a problem where a viscous ferrofluid, surrounded by a nonmagnetic fluid, is subjected to a radial magnetic field in a Hele-Shaw cell. Elasticity comes into play when the fluids are brought into contact, and due to a chemical reaction, the interface separating them becomes a gel-like elastic layer. A perturbative linear stability theory is used to investigate how the combined action of magnetic and elastic forces can lead to the development of smooth, low-amplitude, sinusoidal wrinkles at the elastic interface. In addition, a nonperturbative vortex sheet approach is employed to examine the emergence of highly nonlinear, magnetically driven, wrinkling and folding equilibrium shape structures. A connection between the magnetoelastic shape solutions induced by a radial magnetic field and those produced by nonmagnetic means through centrifugal forces is also discussed.

DOI: [10.1103/PhysRevE.99.022608](https://doi.org/10.1103/PhysRevE.99.022608)

## I. INTRODUCTION

The study of the formation of wrinkled and folded patterns in thin elastic membranes resting on a fluid or on a very soft gel-like substrate has received much attention in recent years [1–4]. Laboratory experiments, numerical simulations, and analytical studies [5–9] show that when an elastic membrane lies on a flat surface of a liquid, the membrane assumes different shapes when compressed laterally. The pattern-forming structures result from the balance of elastic and hydrodynamic forces acting on the membrane. For low compressions, small-amplitude sinusoidal undulations arise at the membrane, creating a periodic wrinkling pattern. If the wrinkled surface is compressed further, then a different type of pattern emerges: The wrinkles increase their amplitude, and the smooth wrinkling is replaced by more convoluted localized structures in the form of a single or multiple folds. If the compression process continues, then the elastic membrane eventually makes contact with itself, giving rise to teardrop-like-shaped folds. It has been recently shown that the fluid-supported elastic sheet problem admits a vast array of multifold states [9] containing both identical and dissimilar folds (for a representative collection of such deformed structures, see, for instance, Figs. 4 and 6 in Ref. [9]).

It is worth noting that, in addition to its intrinsic scientific and academic value, these wrinkling and folding phenomena [1–9] have a large number of practical applications, being observed in various contexts and length scales ranging from the

folding of geological layers [10] to patterns in cell membranes and biological tissues [11–13].

A related fluid-structure system that also involves the interplay of elastic and hydrodynamic forces is the one that deals with elastic capsules (closed monolayers) or elastic vesicles (closed bilayers) [14,15]. Such types of closed membrane arrangements consist of a thin elastic shell enclosing a fluid inside. Interfacial instabilities can be triggered when elastic capsules and vesicles are subjected to external forces. For example, a possible route to exert forces on such closed elastic membranes is through the use of external magnetic fields. This specific shape changing technique requires the presence of a magnetizable material inside the elastic structure. Under such circumstances, the sealed membrane would acquire a magnetic dipole moment, which can be properly manipulated by external magnetic fields.

Experiments using a magnetic field to probe the shape of vesicles filled with a magnetic fluid (a ferrofluid) were performed by Bacri *et al.* more than two decades ago [16]. Ferrofluids [17–20] are stable colloidal suspensions composed of minute, nanometersized magnetic particles dispersed on a nonmagnetic carrier fluid. When a magnetic field is applied, the magnetic forces in the ferrofluid compete with the bending stiffness of the elastic membrane, and the equilibrium shapes of the vesicle are altered. In particular, the external magnetic field tends to elongate the original nearly spherical elastic structure along the field direction, which assumes a prolate shape [16].

Recently, numerical simulations and analytical calculations have been employed to investigate theoretically the deformation of ferrofluid-filled elastic capsules in uniform external magnetic fields [21]. Spheroidal shapes (prolate spheroids) have been found at small and moderate magnetic fields, whereas elongated shapes presenting conical tips have been detected at high magnetic fields. It has also been found

\*pedroanjos@df.ufpe.br

†gabrielcdc@cbpf.br

‡sergio@fis.ufal.br

§jme@df.ufpe.br

that the capsule can develop wrinkling-type instabilities if circumferential compressive stresses arise as a result of the stretching along the direction of the applied magnetic field.

The magnetic closed membrane structures studied experimentally in Ref. [16] and theoretically in Ref. [21], and the encapsulation of magnetic fluids in elastic shells [22] have been proven useful tools in order to allow magnetic tuning of the shapes of giant liposomes (or magnetoliposomes) [23], as well as on probing mechanical and rheological properties of living cells [24] and developing tissues [25].

In spite of the practical usefulness and scientific relevance of the fluid-structure problems involving the interplay of hydrodynamic, elastic, and magnetic forces, the deformed interface morphologies of the ferrofluid-filled elastic membrane systems studied in Refs. [16,21–25] are not as complex and visually striking as the aforementioned wrinkling and folding patterns investigated in Refs. [1–9]. Therefore, a study of the development of sizable wrinkling and folding instabilities in a ferrofluid system that involves the interplay of magnetic and elastic effects is still lacking. This work aims to begin filling this gap in the literature.

Given the complexity of such magnetoelastic pattern-forming situation, in this paper we begin to tackle the problem by considering a simplified theoretical description. First, instead of dealing with the much more complicated, three-dimensional (3D) ferrohydrodynamic fluid-structure problem, we focus on an effectively 2D situation and consider the flow of a viscous ferrofluid droplet, surrounded by a nonmagnetic fluid of negligible viscosity, between two closely spaced glass plates of a Hele-Shaw cell [26–28]. To try to induce changes at the two-fluid interface, we consider the action of a radial magnetic field, applied in the plane of the Hele-Shaw cell [29,30]. Such a radial magnetic field configuration has already been utilized as an experimental tool to examine the formation of interfacial patterns in free surface flows of both miscible and immiscible thin ferrofluid films [31,32]. In addition, as in Refs. [33–38], we consider that the fluid-fluid interface is elastic and has a constant bending rigidity. Experiments in Hele-Shaw cells [39] have shown that such an elastic interface can be produced when the fluids are brought into contact, and a micellar chemical reaction occurs, so that the fluid-fluid boundary becomes an elastic gel-like layer. In this confined geometric setting, the traditional Saffman-Taylor, viscous fingering instability [28] is supplemented by magnetic and elastic interactions, and in principle the ferrofluid droplet could evolve into intricate interfacial patterns containing wrinkles and folds, hopefully as interesting and elaborate as those that arise in Refs. [1–9].

Broadly speaking, our magnetoelastic problem serves as a Hele-Shaw flow sort of counterpart to the compressed, fluid-supported elastic sheet problem studied in Refs. [1–9]. However, we stress that even though our current study is motivated by the wrinkling and folding phenomena that emerge in elastic sheets under compression, a direct equivalence between these two distinct physical problems should not be implied. As a matter of fact, even the theoretical approaches employed to gain access to the complex wrinkling and folding structures are different: While in Refs. [1–9] Lagrangian and Hamiltonian approaches are used by considering compressed membranes subjected to some constraints, here we utilize an

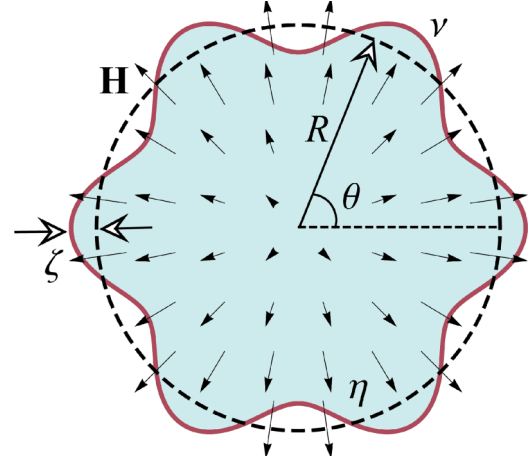


FIG. 1. Schematic illustration (top view) of a magnetic field-induced flow in a Hele-Shaw cell. The cell contains an initially circular viscous ferrofluid droplet of radius  $R$  (dashed curve) and viscosity  $\eta$ , surrounded by a nonmagnetic fluid with negligible viscosity. The fluid-fluid interface is elastic and has a constant bending rigidity  $\nu$ . The system is subjected to an in-plane external magnetic field  $\mathbf{H}$  pointing radially outward. The interplay of magnetic and elastic forces deforms the interface (solid curve), and the interface perturbation amplitude is denoted by  $\zeta = \zeta(\theta, t)$ , where  $\theta$  is the azimuthal angle and  $\zeta \ll R$ .

unconstrained vortex sheet formalism [40,41]. This issue will be further discussed in Sec. III.

The rest of this work is outlined as follows. A perturbative linear stability analysis of the system is presented in Sec. II, unveiling how the combined action of magnetic and elastic effects determine the stability properties of the interface at early stages of the dynamics. Section III indicates how a vortex sheet formalism for Hele-Shaw problems [42,43] can be used to access fully nonlinear, stationary, interface shape solutions, which are obtained when magnetic and elastic forces are exactly matched at the two-fluid interface. A representative collection of such equilibrium shape solutions is presented, revealing the formation of suggestive wrinkling and folding patterns. A parallel between the radial magnetic field-induced shape solutions, and those generated by nonmagnetic means via centrifugal forces is also examined. Finally, our main conclusions and perspectives are summarized in Sec. IV.

## II. LINEAR DYNAMICS OF INTERFACIAL PERTURBATIONS

In this section, we describe analytically and perturbatively the early time dynamics of the interface separating a viscous ferrofluid droplet, surrounded by nonmagnetic fluid of negligible viscosity, considering that they are confined to flow in the narrow gap separating the two parallel glass plates of a Hele-Shaw cell. A top view of the system is represented in Fig. 1. The ferrofluid (nonmagnetic fluid) viscosity is denoted by  $\eta_1 = \eta$  ( $\eta_2 \ll \eta$ ), and the Hele-Shaw cell gap thickness is represented by  $b$ . The fluids are Newtonian and incompressible. The fluid-fluid interface is elastic and has a constant bending rigidity given by  $\nu$ . The system is subjected

to an externally applied radial magnetic field [29,30]

$$\mathbf{H} = \frac{H_0}{L} r \hat{\mathbf{e}}_r, \quad (1)$$

where  $H_0$  is a constant,  $L$  is a characteristic length,  $r$  is the radial distance from the origin of the coordinate system (located at the center of the cell), and  $\hat{\mathbf{e}}_r$  is a unit vector in the radial direction. Such a magnetic field is produced by a pair of identical Helmholtz coils whose electric currents are equal and flow in opposite directions [31,32]. The Hele-Shaw cell is located at the mid-distance between the coils, such that the radial magnetic field is coplanar to it. A magnetic body force  $\sim \nabla H$ , where  $H = |\mathbf{H}|$  is the local magnetic field intensity, acts on ferrofluid pointing in the outward radial direction.

Notice that the consideration of the in-plane radial magnetic field given by Eq. (1) is not simply an academic exercise but something that can be implemented in practice. At first glance, from Eq. (1) and by inspecting Fig. 1 one might think that such a magnetic field configuration does not fulfill the condition of the closure of magnetic field lines (see center of the droplet in Fig. 1). However, it should be stressed that, within the Hele-Shaw cell, the radial magnetic field expressed by Eq. (1) is a 2D limit of a fully 3D magnetic field (the so-called magnetic quadrupole field). This 3D field is created by the two Helmholtz coils having opposite flowing currents, as mentioned earlier. Such a quadrupole magnetic field is indeed divergenceless, and the condition for the closure of the field line is obeyed. Incidentally, this magnetic quadrupole field configuration is of significant practical relevance and has been extensively used to produce magneto-optical traps (MOPs) for neutral atoms and molecules (see, for instance, Refs. [44,45]). At the mid-distance between the coils (where the thin Hele-Shaw cell is located), and for small radial distances, the 3D magnetic quadrupole field reduces to the purely radial 2D field given by Eq. (1) (see Eqs. (A6)–(A9) in Ref. [46]). Within the Hele-Shaw cell, where transversal distances [ $z \sim O(b)$ ] are much smaller than typical radial lengths [ $r \sim O(R)$ ], and the radial component of the quadrupole field is much larger than its transversal counterpart. Under such circumstances, the in-plane field acting in the Hele-Shaw cell is given by Eq. (1). As pointed out in Sec. I, experimental realizations of this radial magnetic setup in ferrofluid systems have been presented in Refs. [31,32].

Since the applied radial magnetic field [Eq. (1)] presents a natural nonzero gradient, we take it as the main local field contribution to the magnetic body force. In our analysis we have not considered the influence of the demagnetizing (or induction) field [17–20]. Within the scope of our problem (in-plane applied magnetic field and relatively low values of the magnetic susceptibility) demagnetizing effects can be safely neglected.

It should be pointed out that a small change in radial magnetic field setup leads to the action of a completely different magnetic field configuration: By using the very same Helmholtz coils apparatus mentioned above, but making the electric currents to flow in the same direction, one obtains a uniform magnetic field which is perpendicular to the Hele-Shaw cell plates [17,18]. The perpendicular magnetic field arrangement has been widely used in Hele-Shaw flow studies of a very popular pattern formation problem in ferrofluids,

known as the labyrinthine instability problem [47–50], where eye-catching and impactful multiply branched structures arise.

Here we underline in a bit more detail the demagnetizing field approximation in confined ferrofluids and the reasons for disregarding demagnetizing field effects in our current radial magnetic field problem in Hele-Shaw cells. In ferrohydrodynamics [17–20,51,52], it is well known that the magnetic body force can be formally expanded in terms of the ferrofluid volume fraction. In fact, the demagnetization expansion is based on an expansion of the magnetic field in terms of the volume fraction and is always valid, provided the volume fraction is not too high (i.e., the magnetic suspensions cannot be too concentrated). This is precisely the regime we consider in this work. In such expansion, the magnetic field strength contributes up to all orders. In this context, the magnetic body force in ferrofluids contains terms produced by the externally applied field, supplemented by correction terms related to the demagnetizing field. The demagnetizing field corrections are proportional to  $(b/R)\chi^2 N_B$  [17–20,47–52], where  $R$  is the radius of the initially circular ferrofluid droplet,  $b$  is the already-defined Hele-Shaw cell gap spacing,  $\chi$  is the magnetic susceptibility of the ferrofluid, and  $N_B$  is a dimensionless magnetic Bond number of the system [in our case, a magnetoelastic number defined by Eq. (11)]. Since within the Hele-Shaw cell approximation,  $b \ll R$ , the ratio  $b/R$  can be arbitrarily small [ $\sim O(10^{-3})$ ] [26–28,47–50]. In addition, the magnetic susceptibility used in this work varies in the range  $10^{-1} < \chi < 1$ , while  $10 < N_B < 10^3$ . For the circumstances of our current work,  $(b/R)\chi^2 N_B$  is of order  $10^{-2}$ . Consequently, the contributions from the demagnetizing field are much smaller than those produced by the applied radial field, and demagnetizing effects can be neglected. We emphasize that this is *not* the case for a ferrofluid droplet subjected to a uniform magnetic field, perpendicular to the plates of a Hele-Shaw cell [47–50]: In this situation, the applied perpendicular field has a zero gradient, and the demagnetizing field effect must be taken in account since it is the first nonzero correction to the magnetic body force. So, contrary to what occurs in our radial magnetic field case, the demagnetizing effects cannot be neglected in the perpendicular field situation and are in fact essential to describe the emergence of the resulting labyrinthine pattern-forming structures.

In the framework of our first-order perturbative theory, the perturbed shape of the interface can be written as  $\mathcal{R}(\theta, t) = R + \zeta(\theta, t)$ , where  $R$  is the radius of the initially circular two-fluid interface and  $\theta$  is the azimuthal angle (Fig. 1). Here  $\zeta(\theta, t) = \sum_{n=-\infty}^{+\infty} \zeta_n(t) \exp(in\theta)$  represents the net interface perturbation with complex Fourier amplitudes  $\zeta_n(t)$  and discrete azimuthal wave numbers  $n$ .

The effectively 2D dynamics of the system can be described by a generalized Darcy's law for the gap-averaged velocity [47–50]

$$\mathbf{v}_j = -\frac{b^2}{12\eta_j} \nabla \Pi_j, \quad (2)$$

where the index  $j$  is 1 for the inner fluid and 2 for the outer one. In Eq. (2) the gap-averaged generalized pressure

is defined as

$$\Pi_j = \frac{1}{b} \int_{-b/2}^{+b/2} [P_j - \Psi] dz = p_j - \psi, \quad (3)$$

where  $P_j$  is the 3D pressure,  $p_j = [\int_{-b/2}^{+b/2} P_j dz]/b$  is the gap-averaged pressure, and

$$\Psi = \mu_0 \int_0^H M dH = \frac{\mu_0 \chi H^2}{2} \quad (4)$$

represents a magnetic pressure [17], with  $\mu_0$  denoting the magnetic permeability of free space. In Eq. (4) we used the linear relationship  $\mathbf{M} = \chi \mathbf{H}$ , with  $M = |\mathbf{M}|$  being the magnetization of the ferrofluid and  $\chi$  its magnetic susceptibility. Note that since the radial magnetic field [Eq. (1)] is independent of  $z$ , we have that the gap-averaged magnetic pressure  $\psi = [\int_{-b/2}^{+b/2} \Psi dz]/b = \Psi$ . Additionally, notice that for the nonmagnetic outer fluid  $\chi = 0$  and  $\Psi = 0$ .

We point out that as in Refs. [17–20,51,52], in our current problem magnetophoresis effects can be neglected. The phenomenon of magnetophoresis [53] occurs when a magnetic field gradient produces a gradient in the magnetic particle concentration. Such a magnetophoretic effect drives magnetic particles to areas of larger magnetic field strength, leading to particle agglomeration where the magnetic field is larger. However, as in Refs. [17–20,51,52] we consider that the concentration of magnetic particles is constant, and magnetophoresis effects are not relevant. As a matter of fact, it has been shown [54] that under typical ferrohydrodynamics circumstances, the characteristic time for the magnetophoresis effect to become relevant is of the order of  $10^5$  s, being much larger than the characteristic time for the viscous dominated, Darcy's law flow that occurs in Hele-Shaw cells (which are of order of seconds). In this case, suspended magnetic particles do not have enough time to move relative to the surrounding nonmagnetic liquid carrier due to the Stokes drag, and magnetophoresis effects can be disregarded.

From Darcy's law Eq. (2) and the incompressibility condition  $\nabla \cdot \mathbf{v}_j = 0$ , it can be verified that the velocity potential  $\phi_j$ , where  $\mathbf{v}_j = -\nabla \phi_j$  obeys Laplace's equation. In the context of Hele-Shaw flows [26,27], our Laplacian problem is completely specified by two boundary conditions at the interface  $r = \mathcal{R}$ . The first one is the augmented Young-Laplace pressure boundary condition [17,18,33–38],

$$(p_1 - p_2)|_{r=\mathcal{R}} = \left[ v \left( \frac{1}{2} \kappa^3 + \kappa_{ss} \right) - \frac{1}{2} \mu_0 (\mathbf{M} \cdot \hat{\mathbf{n}})^2 \right]_{r=\mathcal{R}}, \quad (5)$$

where

$$\kappa = \frac{\mathcal{R}^2 + 2 \left( \frac{\partial \mathcal{R}}{\partial \theta} \right)^2 - \mathcal{R} \frac{\partial^2 \mathcal{R}}{\partial \theta^2}}{\left[ \mathcal{R}^2 + \left( \frac{\partial \mathcal{R}}{\partial \theta} \right)^2 \right]^{3/2}} \quad (6)$$

denotes the interface curvature in the plane of the cell, and the subscripts of  $\kappa$  indicate derivatives with respect to the arclength  $s$ . In addition,  $\hat{\mathbf{n}}$  denotes the unit normal vector at the interface. The first term on the right-hand side of Eq. (5) is related to the pressure jump due to the elasticity of the interface. It is obtained by minimizing the Canham-Helfrich

energy functional [33–38],

$$E = \frac{1}{2} \int v \kappa^2 ds, \quad (7)$$

and represents the simplest model for the elastic response of the interface. The second term on the right-hand side of Eq. (5) is commonly known as the magnetic normal traction term [17,18] and incorporates the influence of the discontinuous normal component of the magnetization at the interface. Notice that as in Refs. [55–57], in contrast to the usual Hele-Shaw cell problem, surface tension effects are neglected in Eq. (5).

The other relevant boundary condition (known as the kinematic boundary condition [26,27]) connects the velocity of the ferrofluid with the motion of the interface itself

$$\frac{\partial \mathcal{R}}{\partial t} \Big|_{r=\mathcal{R}} = \left[ \frac{1}{r^2} \frac{\partial \mathcal{R}}{\partial \theta} \frac{\partial \phi_j}{\partial \theta} - \frac{\partial \phi_j}{\partial r} \right] \Big|_{r=\mathcal{R}}. \quad (8)$$

Equation (8) expresses the fact that the normal components of the fluids velocities are continuous across the interface.

After presenting the equation of motion of the system [Eq. (2)], and the related boundary conditions [Eq. (5) and Eq. (8)], we now present a perturbative linear stability analysis of the problem. In this framing, our primary task is to derive the linear dispersion relation (or the linear growth rate). In order to do that, we define Fourier expansions for the velocity potential and use the kinematic boundary condition (8) to express the Fourier coefficients of  $\phi$  in terms of the Fourier perturbation amplitudes  $\zeta_n$ . Substituting these relations and the pressure jump condition (5) into the modified Darcy's law Eq. (2), always keeping terms up to first-order in  $\zeta$  and Fourier transforming, we find the *dimensionless* equation of motion for the perturbation amplitudes  $\zeta_n$ ,

$$\dot{\zeta}_n = \lambda(n) \zeta_n, \quad (9)$$

where the overdot represents a total time derivative with respect to time and

$$\lambda(n) = |n| \left\{ 2N_B \chi (1 + \chi) + \frac{(n^2 - 1)}{R^5} \left[ \frac{5}{2} - (n^2 + 1) \right] \right\} \quad (10)$$

is the linear growth rate. In Eqs. (9) and (10) lengths and time are rescaled by  $r_0$  and  $(12\eta r_0^5)/(v b^2)$ , respectively, where  $r_0$  is a typical length being on the order of the unperturbed ferrofluid droplet radius  $R$ . Within this dimensionless description the system is conveniently characterized by the magnetic susceptibility  $\chi$  and by a magnetoelastic number,

$$N_B = \frac{\mu_0 H_0^2 r_0^5}{2L^2 v}, \quad (11)$$

which measures the ratio of magnetic to elastic forces [58,59].

By examining Eq. (10) for the linear growth rate, one immediately notices that it is time-independent. Consequently, Eq. (9) can be easily integrated, resulting in the exponential growth (decay) of the linear perturbation amplitudes with time if  $\lambda(n) > 0$  [ $\lambda(n) < 0$ ]. We can also directly verify the dependence of the linear growth rate on mode  $n$ . For the modes that preserve circular shape (i.e.,  $n = 0$  and  $n = 1$ ) we have mode  $n = 0$  (uniform expansion of the circular interface) is marginal

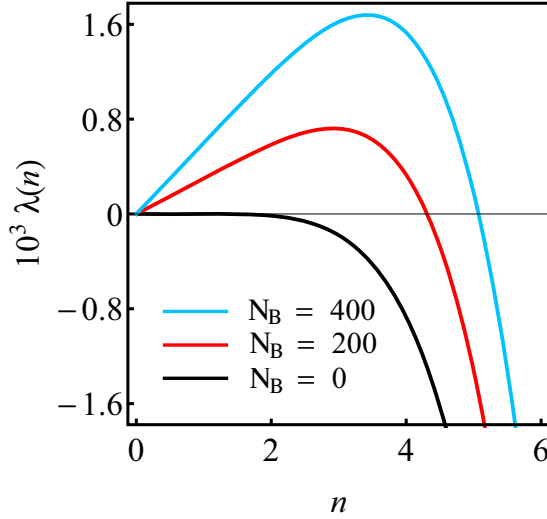


FIG. 2. Linear growth rate  $\lambda(n)$  as a function of the azimuthal wave number  $n$  for  $\chi = 0.5$ , and three values of the magnetoelastic number  $N_B$ : 0, 200, and 400. Here we have that  $R = 1$ .

$[\lambda(n=0) = 0]$ , while mode  $n = 1$  (global off-center shift of the circular interface) is unstable, since  $2N_B\chi(1 + \chi) > 0$ . However, if  $n \geq 2$  the stability of the elastic interface depends on the interplay of the two terms of Eq. (10). Notice that the only destabilizing term in Eq. (10) is the one related to the radial magnetic field (term proportional to  $N_B$ ). On the other hand, the contribution coming from the bending elasticity of the interface [term proportional to  $(n^2 - 1)$ ] acts to restrain interface deformation.

Figure 2 illustrates how the linear growth rate  $\lambda(n)$  varies with mode  $n$  for three increasingly larger values of the magnetoelastic number  $N_B$ , for  $\chi = 0.5$ , and  $R = 1$ . From Fig. 2 the destabilizing role of  $N_B$  becomes quite evident: Larger values of  $N_B$  increase the width of the band of unstable modes as well as the peak location of the curves. Therefore, by manipulating  $N_B$  one can induce deformations at the elastic interface in our magnetoelastic problem.

A useful quantity that can be calculated in closed form from the growth rate expression (10) is the mode of maximum growth rate  $n_{\max}$  [i.e., the one that gives the peak location of the  $\lambda(n)$  curves]. It can be obtained by the condition  $[d\lambda(n)/dn]_{n=n_{\max}} = 0$ , leading to

$$n_{\max} = \frac{1}{2} \sqrt{3 + \sqrt{9 + \frac{8}{3}[4N_B\chi(1 + \chi)R^5 - 3]}}. \quad (12)$$

At the linear level, the closest integer to  $n_{\max}$  provides an estimate for the number of undulations formed at the elastic interface. Note that the number of undulations increases with both  $N_B$  and  $\chi$ .

Another quantity of interest that can be extracted from the linear growth rate (10) is the critical value of the magnetoelastic number at which the  $n$ th mode becomes unstable. This happens when  $\lambda(n) = 0$ , yielding

$$N_B^{\text{crit}}(n) = \frac{(n^2 - 1)}{2\chi(1 + \chi)R^5} \left[ (n^2 + 1) - \frac{5}{2} \right]. \quad (13)$$

These [Eqs. (10)–(13)] are basically the most relevant pieces of information that one can extract at the purely linear level (i.e., stability behavior of a circular elastic interface against small radial magnetic field-induced perturbations).

One additional and interesting issue that can be perceived already at the linear regime is the “rotating Hele-Shaw cell limit” [43]. By this we mean the limit  $\chi \rightarrow 0$  such that the product  $\chi N_B$  remains constant. In this limit the interface behavior of a ferrofluid droplet under a radial magnetic field in a motionless Hele-Shaw cell reverts to the behavior of a nonmagnetic fluid droplet in a rotating Hele-Shaw cell [60,61]. This curious connection between these two apparently unrelated physical systems comes from the fact that in both problems (i.e., magnetically and centrifugally driven cases) the scalar potentials are proportional to  $r^2$ . This limit can be useful to try to link our current magnetoelastic problem to other existing situations in which elastic and centrifugal forces act in the spatially confined environment of a Hele-Shaw cell [62–64].

Within the scope of a perturbative linear theory, the interfacial disturbances must be of small magnitude ( $\zeta \ll R$ ). Moreover, at the linear level the participating Fourier modes  $n$  decouple [as expressed by Eq. (9)]. Thus, at the linear regime each participating mode grows or decays independently of one another. So, essentially, linear analysis offers access to the stability of the interface with regards to the action of a particular, single mode. As a result of these considerations, through a linear description, only small, purely sinusoidal shaped fingers would emerge at the elastic interface. In this sense, linear analysis would be able to make a fair mimic of the onset of the wrinkling instability [1–4], as long as the wrinkles are small, smooth, and described as sinusoidal undulations across the entire elastic boundary. However, as the wrinkles grow in amplitude and their shapes become more complex (not exactly sinusoidal) the linear description fails. By the same token, a perturbative linear approach is not able to reproduce the shape of the rising folds which are more complicated, nonlinear structures that can be nonperiodic and quite convoluted and that can reach large amplitudes. The limitations of a linear analysis are even more serious if one wishes to describe the folding patterns that can be highly localized, and possibly asymmetric, or that present nearly touching, multifold configurations as those that appear in a compressed elastic membrane supported by a fluid substrate [1–9].

### III. FULLY NONLINEAR STATIONARY SHAPES

In Sec. II we have verified that under the action of an applied radial magnetic field, perturbative linear analysis provides useful information about the stability of the elastic interface at initial stages of the Hele-Shaw flow dynamics. In the present section, we go beyond the purely linear level of the pattern formation process and explore important aspects of the fully nonlinear regime in a nonperturbative manner. More specifically, we access highly nonlinear, wrinkling and folding pattern morphologies through the calculation of stationary (equilibrium) solutions of our magnetoelastic problem. In order to accomplish such a task, we employ a technique known as the vortex sheet approach [40–43]. This approach allows a deeper analysis of the magnetoelastic pattern-forming

phenomenon, giving access to its large-deformation limit, including situations in which the interface contacts itself. As in the case of a fluid-supported elastic membrane under compression [1–9], the ability to contemplate the formation of more strongly deformed interfacial structures, and the possible occurrence of self-contact is central to describe the folding instability in our magnetoelastic problem.

Irrespective of the fact that the normal component of the fluids velocities are continuous across the two-fluid interface [26,27] [as expressed by the kinematic boundary condition - Eq. (8)], the tangential components of the velocities are discontinuous when one crosses the fluid-fluid boundary. The vortex sheet formalism explores this jump in the tangential component of the fluid velocity and defines the vortex sheet strength as

$$\Gamma = (\mathbf{v}_2 - \mathbf{v}_1) \cdot \hat{\mathbf{s}}, \quad (14)$$

where  $\mathbf{v}_1$  and  $\mathbf{v}_2$  are the two limiting values of the fluids' velocities at a given point of the interface. In Eq. (14)  $\hat{\mathbf{s}}$  denotes the unit tangent vector along the interface, with  $s$  being the interface arclength. From the generalized Darcy's law Eq. (2), we can say that

$$\eta_1 \mathbf{v}_1 = -\frac{b^2}{12} [\nabla p_1 - \nabla \Psi] \quad (15)$$

for the ferrofluid and

$$\eta_2 \mathbf{v}_2 = -\frac{b^2}{12} \nabla p_2 \quad (16)$$

for the nonmagnetic fluid. Using these expressions, and by subtracting Eq. (16) from Eq. (15), both evaluated at the interface, one obtains

$$\eta_2 \mathbf{v}_2 - \eta_1 \mathbf{v}_1 = -\frac{b^2}{12} [\nabla p_2 - \nabla p_1 + \nabla \Psi]. \quad (17)$$

This equation can be conveniently rewritten in terms of the sum and difference of  $\mathbf{v}_2$  and  $\mathbf{v}_1$  as

$$\frac{(\mathbf{v}_2 - \mathbf{v}_1)}{2} + A \frac{(\mathbf{v}_2 + \mathbf{v}_1)}{2} = \frac{b^2}{12(\eta_1 + \eta_2)} \nabla [(p_1 - p_2) - \Psi], \quad (18)$$

where  $A = (\eta_2 - \eta_1)/(\eta_2 + \eta_1)$  is the viscosity contrast.

Then, by taking the dot product of Eq. (18) with  $\hat{\mathbf{s}}$ , utilizing Eq. (14), and writing the pressure difference  $(p_1 - p_2)$  by using the pressure jump condition [Eq. (5)], we get

$$\begin{aligned} \frac{\Gamma}{2} + A \mathbf{V} \cdot \hat{\mathbf{s}} &= \frac{b^2}{12(\eta_1 + \eta_2)} \nabla \left[ v \left( \frac{1}{2} \kappa^3 + \kappa_{ss} \right) \right. \\ &\quad \left. - \frac{1}{2} \mu_0 (\mathbf{M} \cdot \hat{\mathbf{n}})^2 - \Psi \right] \cdot \hat{\mathbf{s}}, \end{aligned} \quad (19)$$

where  $\mathbf{V} = (\mathbf{v}_1 + \mathbf{v}_2)/2$  is an average velocity of the interface which can be expressed as a Birkhoff integral [40–43]

$$\mathbf{V}(s, t) = \frac{1}{2\pi} P \int ds' \frac{\hat{\mathbf{z}} \times [\mathbf{r}(s, t) - \mathbf{r}(s', t)]}{|\mathbf{r}(s, t) - \mathbf{r}(s', t)|^2} \Gamma(s', t), \quad (20)$$

where  $P$  means a principal-value integral and  $\hat{\mathbf{z}}$  is the unit vector along the direction perpendicular to the cell. Finally, by explicitly writing the expression for  $\Psi$  [using Eqs. (1) and (4)] into Eq. (19), and considering that in our problem the

viscosity of the nonmagnetic fluid is negligible ( $\eta_2 \ll \eta_1 = \eta$ ), and, consequently,  $A = -1$ , a *dimensionless* equation for the vortex sheet strength can be obtained, yielding

$$\frac{\Gamma}{2} = \mathbf{V} \cdot \hat{\mathbf{s}} + \partial_s \left[ \left( \frac{1}{2} \kappa^3 + \kappa_{ss} \right) - N_B r^2 \chi [1 + \chi (\hat{\mathbf{n}} \cdot \hat{\mathbf{e}}_r)^2] \right], \quad (21)$$

where  $\partial_s = \partial/\partial s$  is the derivative along the tangent direction to the interface. The term  $(\hat{\mathbf{n}} \cdot \hat{\mathbf{e}}_r)^2$  in Eq. (21) is reminiscent of the magnetic normal traction contribution in Eq. (5). Notice that Eq. (21) is made dimensionless by using the same rescaling utilized to nondimensionalize Eqs. (9) and (10).

If one intends to describe the time evolution of the interface, then one has to solve numerically a complicated nonlinear integrodifferential equation defined by Eq. (21) and Eq. (20) [40]. However, a significantly simpler vorticity equation is obtained if one focus on the, still fully nonlinear, but stationary solutions of Eq. (21) where magnetic and elastic forces are equally balanced at the interface. In this equilibrium scenario, we have that  $\mathbf{v}_1 = \mathbf{v}_2 = 0$  [42]. By taking  $\mathbf{V} = 0$  in Eq. (21), considering the condition of zero vorticity ( $\Gamma = 0$ ), and writing  $\hat{\mathbf{n}} \cdot \hat{\mathbf{e}}_r = r\theta_s$  [43], we find a nonlinear ordinary differential equation

$$\frac{3}{2} \kappa^2 \kappa_s + \kappa_{sss} - 2N_B \chi [rr_s + \chi r^3 (2r_s \theta_s^2 + r\theta_s \theta_{ss})] = 0, \quad (22)$$

which describes the shape of the elastic two-fluid interface. The determination of a closed-form, exact analytical solution of this shape equation is challenging and poses a rather difficult problem. In this work, we solve Eq. (22) numerically by employing a numerical approach originally presented in Ref. [43]. Such numerical solutions offer a nonperturbative way to gain access to fully nonlinear, stationary interfacial shapes in our magnetoelastic pattern formation problem. Notice that in the rotating Hele-Shaw cell limit [42,43,64] the shape equation [Eq. (22)] reduces to a considerably simpler form

$$\frac{3}{2} \kappa^2 \kappa_s + \kappa_{sss} - 2C rr_s = 0, \quad (23)$$

where  $C = N_B \chi$ .

Here we make a few important remarks about the unconstrained nature of the vortex sheet approach used to obtain the equilibrium magnetoelastic patterns presented in this work. This issue was briefly discussed at the end of Sec. I, and it is now discussed further. The majority of the studies that look for equilibrium shape solutions for the problem of a fluid-supported elastic membrane under compression employ Lagrangian, Hamiltonian, and rod-theory-based methods (see, for example, Refs. [6–9]). In framework of these theoretical approaches, one essentially writes down the energy functional for the system, taking into account some constraints and boundary conditions. Usually, membranes are considered as inextensible objects and therefore must present a fixed length (that can be either finite or infinite), being subjected to clamped, periodic, or far-field boundary conditions. Such an energy functional is then minimized, leading to a differential equation whose solution provides the desired equilibrium structures. Nevertheless, as one can find out by inspecting

Refs. [1–9], the derivation and solution of such differential equations are not always straightforward.

In this work, we follow an alternative route and derive the differential equation for the equilibrium magnetoelastic shapes by employing an unconstrained vortex sheet approach [40–43]. This theoretical tool offers a particularly simple method to obtain the differential equation that governs the shape of the stationary magnetoelastic patterns [Eq. (22)], allowing one to probe the morphology of such fully nonlinear shapes. However, in contrast to the theoretical approach adopted in Refs. [6–9], the vortex sheet technique imposes no constraints over the contour lengths and areas of the resulting closed and non-self-crossing equilibrium structures. Nonetheless, it should be emphasized that the unconstrained nature of the vortex sheet approach does not obscure its most convenient feature: its ability to allow proper access to prominent fully nonlinear morphological elements of the resulting equilibrium magnetoelastic patterns. The formulation of a constrained version of the vortex sheet approach is certainly an appealing and challenging research topic but goes beyond the scope of our current work.

Before proceeding, we briefly discuss how to conciliate the establishment of the problem of determining stationary shapes for the magnetoelastic situation [governed by Eq. (22)], with the instability related to the rigid translational motion of the circular ferrofluid droplet [mode  $n = 1$  in the linear growth rate given by Eq. (10)]. Of course, the displacement mode  $n = 1$  is just one of the many possible unstable modes of the problem; however, it is the one directly connected to the rigid motion of the droplet, something that in principle could jeopardize the notion of a truly stationary solution. From a general point of view in nonlinear dynamics [65], it is important to know all fixed points of the dynamics, either stable or unstable, even if the unstable ones may not be easily observable. The effect of the unstable ones in the dynamics may be directly observable as a slowing down when the system passes nearby a steady solution (which may be forced through the choice of initial conditions). In the case of the displacement mode  $n = 1$ , in particular if the initial condition is carefully well centered, it may take a long time to excite the displacement mode by noise. Note, for instance, that in experiments of centrifugal fingering of nonmagnetic fluids in Hele-Shaw cells [60,61], as well as for experiments of free surface flows with ferrofluids under radial magnetic fields [31,32], the mode  $n = 1$  is also unstable, but the experiments have been carried out without any observable, significant global displacement of the droplet. By the way, stationary solutions have already been determined for the nonmagnetic centrifugally driven fingering problem in Hele-Shaw cells [42,43] and for the nonelastic case of a confined ferrofluid droplet subjected to a radial magnetic field [29]. In both cases, it has been shown that stationary solutions are indeed of relevance to reveal important morphological and dynamical properties of these systems. Based on these facts, we can say that there is no incompatibility between the instability of mode  $n = 1$  and the establishment of stationary solutions via the vortex sheet approach.

At this point we turn to the discussion of a representative collection of fully nonlinear pattern-forming solutions of the nonlinear differential equation (22). We stress that all patterns

shown in this section are stationary (equilibrium) shapes, corresponding to the situation in which magnetic and elastic forces are equally balanced at the interface. A number of important morphological features of the stationary solutions can be obtained by the numerical evaluation of Eq. (22) via the manipulation of the relevant control parameters of the problem, namely  $N_B$  and  $\chi$ . Once these physical parameters are chosen, we try various different sets of initial conditions and search numerically for acceptable (i.e., physically relevant) patterns whose boundaries must be closed and non-self-crossing. For a thorough discussion about the numerical approach used to solve the type of differential equation given in Eq. (22), as well as the non-self-crossing nature and commensurability of the stationary pattern-forming solutions, we refer the interested reader to Refs. [43,66–68].

We begin our analysis by inspecting Fig. 3. In the top row [Figs. 3(a)–3(c)] we have a collection of representative stationary solutions for the problem considering that the magnetoelastic number  $N_B = 48$ , while the magnetic susceptibility of the ferrofluid droplet takes increasingly larger values: (a)  $\chi = 0.5731$ , (b)  $\chi = 0.6271$ , and (c)  $\chi = 0.6547$ . On the other hand, in the bottom row [Figs. 3(d)–3(f)] we represent the corresponding rotating Hele-Shaw cell limit patterns to those depicted in Figs. 3(a)–3(c) by keeping the product  $\chi N_B$  constant and by setting  $\chi \rightarrow 0$ .

By scrutinizing the top panels of Fig. 3 we observe that these magnetoelastic patterns present a quite distinctive morphology: Each equilibrium pattern presents an envelope structure in the form of a concave-shaped “polygon” having a given  $N$ -fold symmetry (with  $N = 3, 4$ , and  $5$ ). Moreover, one notices the formation of a fairly wrinkled perimeter along the elastic interface of such  $N$ -gons. It is also evident that by increasing the value of  $\chi$ , the result is an increase in both  $N$  and in the number of the tiny wrinkles that emerge at the elastic interface. Another noteworthy observation is the fact that, in contrast to the wrinkles formed on the curved edges of the  $N$ -fold polygons (these wrinkles are mostly sinusoidal-like), the small size fingered shapes formed at the vertices look more like folds (they are more deformed and present a teardrop-like shape). The patterns depicted in Fig. 3 resemble the wrinkled, serpentine-like elastic structures that arise in some biological systems (see, e.g., Fig. 1(b) in Ref. [4]). They are also similar to some of the wrinkled shapes that appear in the problem of a compressed fluid-supported elastic sheet [1–9].

As a matter of fact, as  $\chi$  is increased one notices that these isolated folds located at the vertices become more distorted, favoring the contact of the interface with itself [see bottom part of Fig. 3(c)]. We attribute such a behavior to the fact that at the vertices one reaches the largest radial distances from the ferrofluid droplet center, maximizing the strength of the applied magnetic field in these outermost locations. Higher magnetic field intensities tend to induce stronger local interface deformation, facilitating interface self-contact. Folding formation and tendency toward self-contact are also favored by the action of the magnetic traction term in the ferrofluid [see second term on the right-hand side of Eq. (5)], and the term involving  $(\hat{\mathbf{n}} \cdot \hat{\mathbf{e}}_r)^2$  in Eq. (21)]: The magnetic traction term is maximized as  $\hat{\mathbf{n}}$  is collinear to  $\hat{\mathbf{e}}_r$ , pushing more ferrofluid into the folds located near the vertices. These folds then experience large magnetic forces which push the

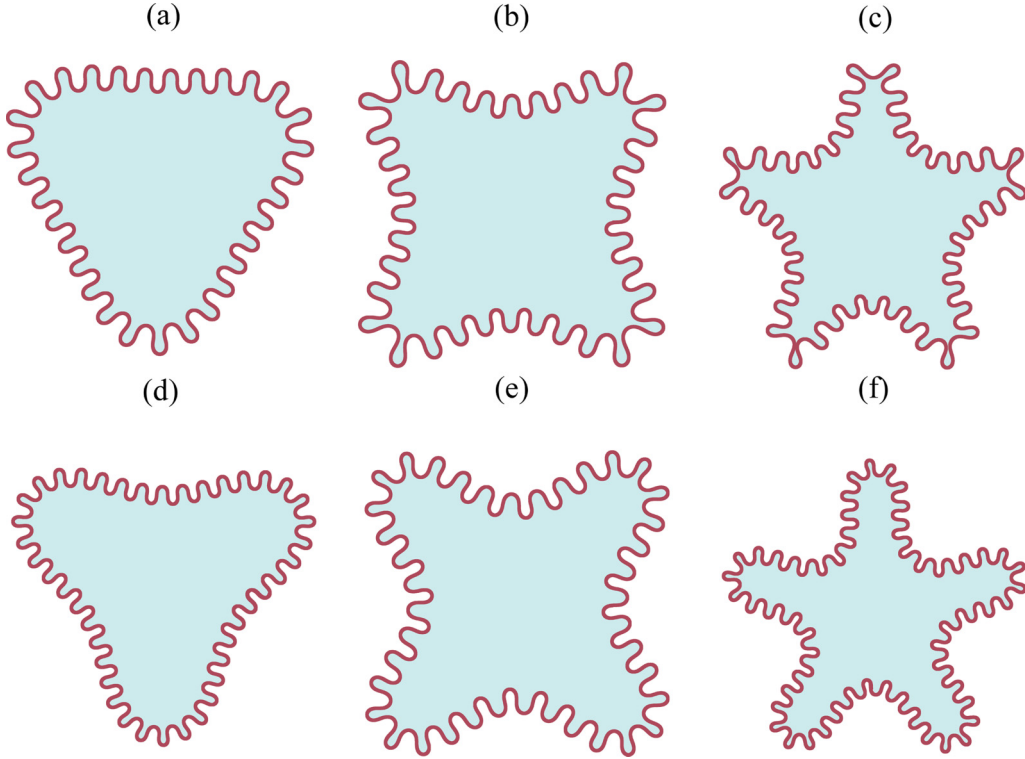


FIG. 3. Top panels: Gallery of representative magnetoelastic patterns for  $N_B = 48$  and three increasing values of the magnetic susceptibility: (a)  $\chi = 0.5731$ , (b)  $\chi = 0.6271$ , and (c)  $\chi = 0.6547$ . Bottom panels: Rotating Hele-Shaw cell limit patterns corresponding to the structures depicted in the top panel, where (d) corresponds to (a), (e) to (b), and (f) to (c). The patterns in the bottom panels are obtained by keeping the product  $\chi N_B$  constant and by taking the limit  $\chi \rightarrow 0$ .

folds' tips further along the radial outward direction, ultimately favoring interface self-contact. In closing, we can say that Figs. 3(a)–3(c) reveal the emergence of peculiar magnetoelastic pattern-forming structures in which smooth, sinusoidal equispaced wrinkles and deformed, localized folds may coexist.

On the other hand, by examining the bottom panels of Fig. 3 we find the rotating Hele-Shaw cell limit patterns that correspond to the magnetoelastic structures illustrated in the top panels. First, it is indeed true that the nonmagnetic patterns depicted in Figs. 3(d)–3(f) are not dramatically different from the magnetoelastic ones shown in Figs. 3(a)–3(c). After all, they are also characterized by the formation of  $N$ -fold polygonlike shapes that present a number of small wrinkled structures along their perimeters. Nevertheless, a closer look reveals that there exist some important differences. The most apparent dissimilarity is the fact that, differently from what is seen in the top panels of Fig. 3, the tips of the fingered envelope structures (located near the vertices of the polygons) in the bottom panels of Fig. 3 are wider and rounded. Furthermore, in the rotating patterns, despite the presence of regular sinusoidal wrinkles, we do not verify the formation of teardrop-like folds near the polygon vertices. In addition, interface self-contact is not observed. These differing morphological features are simply due to the absence of the magnetic traction term contribution in the rotating Hele-Shaw cell limit, in which  $\chi \rightarrow 0$ . So, in the rotating Hele-Shaw cell limit patterns illustrated in Figs. 3(d)–3(f) we observe the favored formation of wrinkles in detriment to

the creation of folds. These findings are consistent with the results obtained in Ref. [64] where similar serpentine interface patterns (their family I which presents no self-contact) have been found in the nonmagnetic centrifugally driven elastic fingering problem.

Another situation of interest refers to the response of the patterns to considerably larger values of the magnetoelastic number  $N_B$ , while the magnitudes of the magnetic susceptibility  $\chi$  are significantly smaller than the equivalent values already considered in Fig. 3. This situation is investigated in Fig. 4. The top panels [Figs. 4(a)–4(c)] depict representative interfacial patterns generated by taking  $N_B = 1143$ , and three magnitudes of the susceptibility: (a)  $\chi = 0.0538$ , (b)  $\chi = 0.0729$ , and (c)  $\chi = 0.125$ . Similarly to what we have in Fig. 3, in the bottom panels of Fig. 4 [Figs. 4(d)–4(f)] we display the rotating Hele-Shaw cell limit patterns that are equivalent to the magnetoelastic structures portrayed in the top panels.

Now, just by quickly inspecting Fig. 4 one can readily tell that the magnetoelastic patterns shown in the top panels are significantly different from their nonmagnetic counterparts illustrated in the bottom panels. In the top panels we verify the formation of highly deformed pattern-forming structures presenting strongly folded fingers of different sizes and thicknesses. When  $\chi$  is increased one notices an increase in the number of folded fingers. It is also apparent that the interface tends to make contact to itself for larger values of  $\chi$  [Fig. 4(c)]. It is curious to see that, despite their morphological complexity, the patterns shown in Figs. 4(a)–4(c) exhibit a

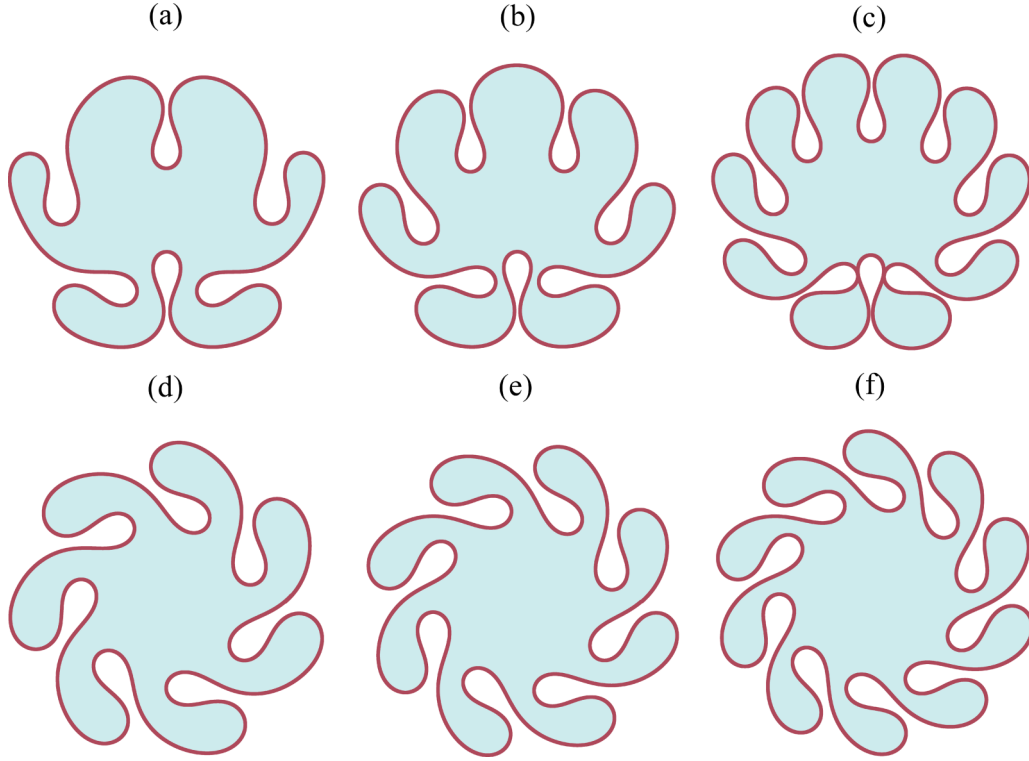


FIG. 4. Top panels: Gallery of representative magnetoelastic patterns for  $N_B = 1143$ , and three increasing values of the magnetic susceptibility: (a)  $\chi = 0.0538$ , (b)  $\chi = 0.0729$ , and (c)  $\chi = 0.125$ . Bottom panels: Rotating Hele-Shaw cell limit patterns corresponding to the structures depicted in the top panels, where (d) corresponds to (a), (e) to (b), and (f) to (c). The patterns on the bottom panels are obtained by keeping the product  $\chi N_B$  constant and by taking the limit  $\chi \rightarrow 0$ .

clear reflection symmetry along the vertical direction: while the folds on the right bend in the counterclockwise direction, the folds on the left part of each pattern are bent in the clockwise direction. Invaginated equilibrium morphologies amusingly similar to the folded structures disclosed in Figs. 4(a)–4(c) arise when an elastic membrane is confined in rigid, cylindrical and spherical containers [69]. Moreover, equilibrium shapes that fold inwards analogous to the magnetoelastic patterns illustrated in the top panels of Fig. 4 also occur in the packing problem of a thin elastic planar ring confined within another shorter flexible ring [70].

A quite distinct set of patterns is unveiled in the bottom panels of Fig. 4, when one considers the rotating Hele-Shaw cell limit of the magnetoelastic situations presented in the top panels. In Figs. 4(d)–4(f) one observes the formation of peculiar swirling patterns. Once again, by enlarging  $\chi$  one ends up producing patterns presenting a larger number of bent folds. Additionally, by increasing  $\chi$  the bases of the bent folds get narrower and narrower, ultimately favoring the self-contact of the elastic interface. Intriguingly, in contrast to what happened in the patterns shown in the top panels, in the bottom panels the patterns are all bent in the same (counterclockwise) direction. Hence, instead of having a reflection symmetry (as the structures in the top panels), the patterns in the bottom panels possess a rotational symmetry. Despite of these interesting findings, the physics underlying this symmetry-breaking behavior when one passes from the magnetoelastic to the centrifugally induced fingering case is nontrivial, still not well understood, and requires additional study. It is worth

noting that similar type of bent finger shapes arise when elastic wires fold in the confined geometry of motionless [71,72] and rotating [62,63] Hele-Shaw cells. In addition, the swirling nonmagnetic patterns shown in Figs. 4(d)–4(f) are analogous to the structures obtained in families II and III in Ref. [64]. Finally, we point out that the folded structures displayed in Fig. 4 have no apparent direct match with the folding patterns normally found in the problem of a laterally compressed elastic sheet lying on a fluid substrate studied in Refs. [1–9].

Note that there is no contradiction involved in the fact of obtaining convoluted shapes from the action of a simple, purely radial, applied magnetic field. The fully nonlinear shapes illustrated in Figs. 3–5 are a result of complicated nonlinear couplings including magnetic and elastic forces, as expressed in the nonlinear ordinary differential equation given by Eq. (22). The interaction of the radial applied field (that naturally has a nonzero gradient), the magnetic traction contribution, plus the nontrivial elastic dependence of the elastic force term in Eq. (5) select the perturbation modes in such a intricate way, generating patterns that can break the initial radial symmetry of the problem. Therefore, despite the simplicity of the radial applied field [Eq. (1)], quite complex pattern-forming shapes can arise at the nonlinear regime.

It should be pointed out that we have searched for other types of pattern-forming structures within and beyond the range of the parameters  $N_B$  and  $\chi$  considered in Figs. 3 and 4, but have not found any other significantly distinct kinds of patterned morphologies other than the ones already presented

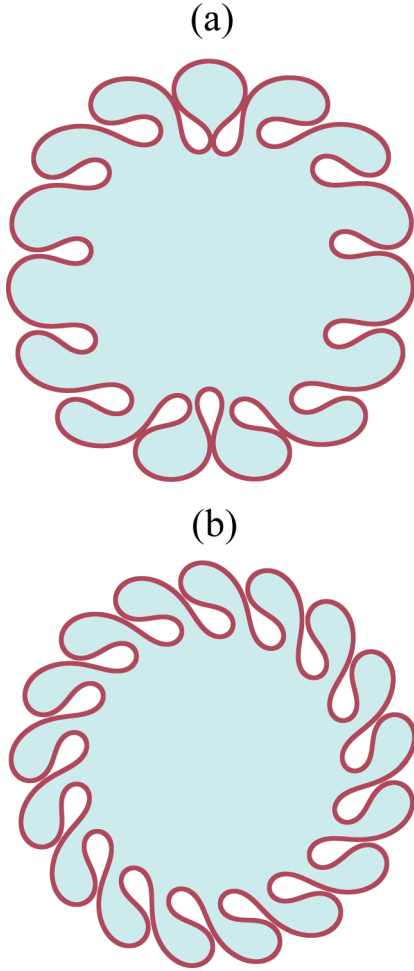


FIG. 5. (a) Representative magnetoelastic pattern for  $N_B = 929$ , and  $\chi = 0.1794$ ; (b) Rotating Hele-Shaw cell limit pattern corresponding to the structure depicted in (a), produced by keeping the product  $\chi N_B$  constant and by taking the limit  $\chi \rightarrow 0$ .

in this work. Representative examples of such slightly different patterns are illustrated in Fig. 5 which presents structures morphologically related to those shown in Fig. 4. It should be stressed that, despite of using various combinations of  $N_B$  and  $\chi$ , we had no success in finding other types of serpentine-like patterns that were dramatically different from those already illustrated in Fig. 3.

Figure 5(a) discloses a magnetoelastic pattern obtained for  $N_B = 929$  and  $\chi = 0.1794$ , and Fig. 5(b) exhibits the corresponding rotating Hele-Shaw cell limit structure. The most evident aspect of the patterns plotted in Fig. 5 is the verification that they are morphologically more complex than the shapes presented in Fig. 4. For instance, when one compares the magnetoelastic pattern depicted in Fig. 5(a) with the equivalent magnetoelastic structure depicted in Fig. 4(c) one observes that in Fig. 5(a) we have more fingers, and the occurrence of more interface self-contact events. It is worthwhile to note that the rotating Hele-Shaw cell limit shape displayed in Fig. 5(b) is also more intricate than the analogous structures obtained in Fig. 4. Namely, the swirling pattern in Fig. 5(b) has many more fingers than the structure appearing in Fig. 4(f). Additionally, in Fig. 5(b) the folded

fingers are about to touch one another, and in Fig. 4(f) the fingers keep a distance from each other.

One more subtle, but still noticeable feature of the magnetoelastic pattern shown in Fig. 5(a) is the fact that it is not completely reflection-symmetric with respect to a vertical line that equally divides this magnetoelastic structure in two sides (i.e., left and right). But in fact, an almost imperceptible reflection asymmetry can be verified. Moreover, contrary to what has been observed in Fig. 4(c), in the magnetoelastic pattern shown in Fig. 5(b) fingers located on the same side (left or right) of the structure are bent in opposite directions (in Fig. 4(c), once you pick a side, all fingers bend in the same direction). It is worth noticing that asymmetric folding patterns (containing distorted folds) have also been identified in Ref. [8] (see their Fig. 4) and in Ref. [9] (see their Fig. 6) in the study of equilibrium shapes of elastic sheets over a liquid substrate.

#### IV. CONCLUSIONS AND PERSPECTIVES

In this paper we have studied an effectively 2D, magnetoelastic analog of the 3D nonmagnetic problem of a fluid-supported elastic membrane under compression. Specifically, we have considered a situation in which a viscous ferrofluid droplet, surrounded by a nonmagnetic fluid of negligible viscosity, is confined in a Hele-Shaw cell and subject to an in-plane, nonuniform external magnetic field pointing radially outward. In addition, we assume that, due to a chemical reaction at the fluid-fluid boundary, the two-fluid interface becomes a thin elastic layer. In this setting, we analyzed the possibility for the appearance of magnetically induced wrinkled and folded structures at the two-fluid interface.

By employing a perturbative linear stability theory we have examined the onset of the pattern formation process. We derived the linear dispersion relation of the problem which reveals the interplay of magnetic and elastic effects: While the radial magnetic field destabilizes the interface, elastic bending forces act to restrain interface disturbances. The net effect at the linear stage is the possibility for the development of a regular pattern of small sinusoidal undulations, characterizing the emergence of magnetically activated wrinkles at the interface. However, linear stability analysis is unable to either predict or capture the formation of much more convoluted structures that may arise at the interface in the form of single or multiple folds.

In order to have access to the creation of large-amplitude, highly nonlinear folded structures, we resorted to the vortex-sheet formalism. By utilizing such a nonperturbative theoretical tool, we derived a nonlinear ordinary differential equation for the stationary pattern-forming shape solutions. Such equilibrium structures correspond to the situation in which magnetic and elastic forces are exactly balanced at the interface. A representative collection of possible patterns has been found. The first class of interface morphologies reveals the formation of polygon-shaped patterns having multiple, tiny wrinkles disposed in a serpentine-like manner. As the magnetic susceptibility is increased, one finds the coexistence of sinusoidal wrinkles and teardrop-like shaped folds. Such a coexistence tends to disappear when the magnetic susceptibility approaches to zero (i.e., in the rotating

Hele-Shaw cell limit), favoring the sole formation of sinusoidal wrinkles.

A second type of characteristic pattern-forming arrangement displays the uprising of complex-shaped, high-amplitude folded structures at the interface. These invaginated folding patterns present an evident reflection symmetry, exhibiting folds that can bend in the clockwise direction in one side of the pattern, or in the counterclockwise direction on the opposite side of the structure. Large values of the susceptibility facilitate the formation of multifold shapes in which the interface can make contact with itself. On the other hand, a completely different set of patterns is obtained in the rotating Hele-Shaw cell limit, where rotationally symmetric, swirling shapes arise in which all folds bend in the same direction.

This work presents theoretical results that have not yet been subjected to the scrutiny of laboratory experiments and fully nonlinear, time-dependent numerical simulations. In particular, it would be of interest to examine the time evolution of the elastic ferrofluid interface from the onset of the linear instability where smooth sinusoidal wrinkles arise, up until the point in which highly nonlinear, intricate folds are formed. As far as numerical simulations are concerned, the time evolution of the magnetoelastic patterns examined here could be described by the integro-differential equation for the vortex sheet strength given by Eq. (21). We plan to tackle this more complicated problem in the future by employing boundary integral numerical techniques as those developed in Refs. [73,74].

It would also be worth it to investigate variants of our current magnetoelastic problem, by considering ferrofluid

droplets subjected to other magnetic field configurations: for instance, a uniform magnetic field perpendicular to the Hele-Shaw cell plates [47–50], or a rotating magnetic acting in the plane of the cell [58]. An additional extension of the present work is the study of the influence of magnetic and elastic forces on a droplet of a more complex magnetic fluid, such as a magnetorheological fluid [75], having an elastic boundary. In this last case, important rheological effects like magnetic field-induced yield-stress could be monitored by external magnetic fields, probably leading to still unexplored wrinkled and folded morphologies.

Our basic understanding of the radial magnetic field-induced magnetoelastic problem proposed in this work is still in its early stages, and many relevant questions remain unanswered. For instance: are other classes of pattern-forming shapes possible? Is it feasible to find exact stationary solutions for the shape equation (22) analytically? If so, how about the stability of such exact analytic solutions? Of course, answering these types of questions, and making further predictions about the large-amplitude pattern shape deformations is nontrivial, mainly due to intrinsic complications regarding geometric nonlinearities. We hope this work will stimulate further studies that might eventually lead to a better comprehension of these challenging, unresolved issues.

#### ACKNOWLEDGMENTS

J.A.M. thanks CNPq (Brazilian Research Council) for financial support under Grant No. 304821/2015-2. This paper has benefited from useful discussions with Jaume Casademunt.

- 
- [1] J. Genzer and J. Groenewold, Soft matter with hard skin: From skin wrinkles to templating and material characterization, *Soft Matter* **2**, 310 (2006).
  - [2] B. Li, Y.-P. Cao, X.-Q. Feng, and H. Gao, Mechanics of morphological instabilities and surface wrinkling in soft materials: A review, *Soft Matter* **8**, 5728 (2012).
  - [3] F. Brau, P. Damman, H. Diamant, and T. A. Witten, Wrinkle to fold transition: Influence of the substrate response, *Soft Matter* **9**, 8177 (2013).
  - [4] R. Zhao and X. Zhao, Multimodal surface instabilities in curved film-substrate structures, *AIME J. Appl. Mech.* **84**, 081001 (2017).
  - [5] L. Pocivavsek, R. Dellsy, A. Kern, S. Johnson, B. Lin, K. Y. C. Lee, and E. Cerda, Stress and fold localization in thin elastic membranes, *Science* **320**, 912 (2008).
  - [6] H. Diamant and T. A. Witten, Compression Induced Folding of a Sheet: An Integrable System, *Phys. Rev. Lett.* **107**, 164302 (2011).
  - [7] O. Oshi, F. Brau, and H. Diamant, Wrinkles and folds in a fluid-supported sheet of finite size, *Phys. Rev. E* **91**, 052408 (2015).
  - [8] G. R. Marple, P. K. Purohit, and S. Veerapaneni, Equilibrium shapes of planar elastic membranes, *Phys. Rev. E* **92**, 012405 (2015).
  - [9] L. Gordillo and E. Knobloch, Fluid-supported elastic sheet under compression: Multifold solutions, [arXiv:1802.09624v1](https://arxiv.org/abs/1802.09624).
  - [10] P. J. Hudleston and S. H. Treagus, Information from folds: A review, *J. Struct. Geol.* **32**, 2042 (2010).
  - [11] S. T. Milner, J.-F. Joanny, and P. Pincus, Buckling of Langmuir monolayers, *Europhys. Lett.* **9**, 495 (1989).
  - [12] M. Kucken and A. C. Newell, Fingerprint formation, *J. Theor. Biol.* **235**, 71 (2005).
  - [13] T. Tallinen, J. S. Biggins, and L. Mahadevan, Surface Sulci in Squeezed Soft Solids, *Phys. Rev. Lett.* **110**, 024302 (2013).
  - [14] D. R. Nelson, T. Piran, and S. Weinberg, *Statistical Mechanics of Membranes and Surfaces*, 2nd ed. (World Scientific, Singapore, 2004).
  - [15] H. F. Nijhout, L. Nadel, and D. L. Stein, *Pattern Formation in Physical and Biological Systems* (CRC Press, Boca Raton, FL, 2018).
  - [16] J.-C. Bacri, V. Cabuil, A. Cebers, C. Menager, and R. Perzynski, Flattening of ferro-vesicle undulations under a magnetic field, *Europhys. Lett.* **33**, 235 (1996).
  - [17] R. E. Rosensweig, *Ferrohydrodynamics* (Cambridge University Press, Cambridge, UK, 1985).
  - [18] E. Blums, A. Cebers, and M. M. Maiorov, *Magnetic Fluids* (de Gruyter, New York, 1997).

- [19] D. Andelman and R. E. Rosensweig, Modulated phases: Review and recent results, *J. Phys. Chem. B* **113**, 3785 (2009).
- [20] J.-C. Bacri and F. Elias, in *Morphogenesis: Origins of Patterns and Shapes*, edited by P. Bourguin and A. Lesne (Springer, New York, 2011).
- [21] C. Wischniewski and J. Kierfeld, Spheroidal and conical shapes of ferrofluid-filled capsules in magnetic fields, *Phys. Rev. Fluids* **3**, 043603 (2018).
- [22] S. Neveu-Prin, V. Cabuil, R. Massart, P. Escaffre, and J. Dussaud, Encapsulation of magnetic fluids, *J. Magn. Magn. Mater.* **122**, 42 (1993).
- [23] O. Sandre, C. Ménager, J. Prost, V. Cabuil, J.-C. Bacri, and A. Cebers, Shape transitions of giant liposomes induced by an anisotropic spontaneous curvature, *Phys. Rev. E* **62**, 3865 (2000).
- [24] C. Wilhelm, F. Gazeau, and J.-C. Bacri, Magnetic micromanipulation in the living cell, *Europhys. News* **36**, 89 (2005), and references therein.
- [25] F. Serwane, A. Mongera, P. Rowghanian, D. A. Kealhofer, A. A. Lucio, Z. M. Hockenbery, and O. Campàs, In vivo quantification of spatially-varying mechanical properties in developing tissues, *Nat. Meth.* **14**, 181 (2017).
- [26] G. M. Homsy, Viscous fingering in porous media, *Annu. Rev. Fluid Mech.* **19**, 271 (1987).
- [27] K. V. McCloud and J. V. Maher, Experimental perturbations to Saffman-Taylor flow, *Phys. Rep.* **260**, 139 (1995).
- [28] P. G. Saffman and G. I. Taylor, The penetration of a fluid into a porous medium or Hele-Shaw cell containing a more viscous liquid, *Proc. R. Soc. Lond. Ser. A* **245**, 312 (1958).
- [29] R. M. Oliveira, J. A. Miranda, and E. S. G. Leandro, Ferrofluid patterns in a radial magnetic field: Linear stability, nonlinear dynamics, and exact solutions, *Phys. Rev. E* **77**, 016304 (2008).
- [30] P. H. A. Anjos, S. A. Lira, and J. A. Miranda, Fingering patterns in magnetic fluids: Perturbative solutions and the stability of exact stationary shapes, *Phys. Rev. Fluids* **3**, 044002 (2018).
- [31] C.-Y. Chen, Y.-S. Yang, and J. A. Miranda, Miscible ferrofluid patterns in a radial magnetic field, *Phys. Rev. E* **80**, 016314 (2009).
- [32] C.-Y. Chen, W.-L. Wu, and J. A. Miranda, Magnetically induced spreading and pattern selection in thin ferrofluid drops, *Phys. Rev. E* **82**, 056321 (2010).
- [33] P. B. Canham, The minimal energy of bending as a possible explanation of the bioconcave shape of the human red blood cell, *J. Theor. Biol.* **26**, 61 (1970).
- [34] W. Helfrich, Elastic properties of lipid bilayers: Theory and possible experiments, *Z. Naturforsch. C* **28**, 693 (1973).
- [35] W. Helfrich, Size distributions of vesicles: The role of the effective rigidity of membranes, *J. Phys.* **47**, 321 (1986).
- [36] O.-Y. Zhong-can and W. Helfrich, Bending energy of vesicle membranes: General expressions for the first, second, and third variation of the shape energy and applications to spheres and cylinders, *Phys. Rev. A* **39**, 5280 (1989).
- [37] A. Nagilla, R. Prabhakar, and S. Jadhav, Linear stability of an active fluid interface, *Phys. Fluids* **30**, 022109 (2018).
- [38] T. R. Powers, Dynamics of filaments and membranes in a viscous fluid, *Rev. Mod. Phys.* **82**, 1607 (2010).
- [39] T. Podgorski, M. C. Sostarecz, S. Zorman, and A. Belmonte, Fingering instabilities of a reactive micellar interface, *Phys. Rev. E* **76**, 016202 (2007).
- [40] G. Tryggvason and H. Aref, Numerical experiments on Hele-Shaw flow with a sharp interface, *J. Fluid Mech.* **136**, 1 (1983).
- [41] G. Birkhoff, Taylor instability and laminar mixing, Los Alamos Scientific Laboratory Technical Report No. LA-1862, pp. 1–76, 1954 (unpublished). See also, G. Birkhoff, Taylor instability: appendices to Report LA-1862, Los Alamos Scientific Laboratory Technical Report No. LA-1927, pp. 1–91, 1956 (unpublished).
- [42] E. Álvarez-Lacalle, J. Ortín, and J. Casademunt, Nonlinear Saffman-Taylor Instability, *Phys. Rev. Lett.* **92**, 054501 (2004).
- [43] E. S. G. Leandro, R. M. Oliveira, and J. A. Miranda, Geometric approach to stationary shapes in rotating Hele-Shaw flows, *Physica D* **237**, 652 (2008).
- [44] T. H. Bergeman, G. Erez, and H. J. Metcalf, Magnetostatic trapping field for neutral atoms, *Phys. Rev. A* **35**, 1535 (1987).
- [45] J. G. E. Harris, R. A. Michniak, S. V. Nguyen, W. C. Campbell, D. Egorov, S. E. Maxwell, L. D. van Buuren, and J. M. Doyle, Deep superconducting magnetic traps for neutral atoms and molecules, *Rev. Sci. Instrum.* **75**, 17 (2004).
- [46] See, for instance, T. P. Meyrath, Experiments with Bose-Einstein condensation in an optical box, Ph.D. thesis, The University of Texas at Austin, 2005, pp. 167–169.
- [47] A. O. Tsebers and M. M. Maiorov, Magnetostatic instabilities in plane layers of magnetizable liquids, *Magnetohydrodynamics* (N.Y.) **16**, 21 (1980).
- [48] A. O. Tsebers, Dynamics of magnetostatic instabilities, *Magnetohydrodynamics* (N.Y.) **17**, 113 (1981).
- [49] S. A. Langer, R. E. Goldstein, and D. P. Jackson, Dynamics of labyrinthine pattern formation in magnetic fluids, *Phys. Rev. A* **46**, 4894 (1992).
- [50] D. P. Jackson, R. E. Goldstein, and A. O. Cebers, Hydrodynamics of fingering instabilities in dipolar fluids, *Phys. Rev. E* **50**, 298 (1994).
- [51] M. Igonin, Hydrodynamic instabilities of miscible and immiscible magnetic fluids in a Hele-Shaw cell, Ph.D. thesis, D. Diderot University Paris 7, 2004.
- [52] M. Igonin and A. Cebers, Labyrinthine instability of miscible magnetic fluids, *Phys. Fluids* **15**, 1734 (2003).
- [53] M. I. Shliomis, Convective instability of magnetized ferrofluids: Influence of magnetophoresis and Soret effect, in *Thermal Nonequilibrium Phenomena in Fluid Mixtures*, Lecture Notes in Physics Vol. 584, edited by W. Kohler and S. Wiegand (Springer, Berlin, 2002), pp. 355–371.
- [54] M. Liu and K. Sierstadt, Thermodynamics, electrodynamics, and ferrofluid dynamics, in *Colloidal Magnetic Fluids*, Lecture Notes in Physics Vol. 763, edited by S. Odenbach (Springer, Berlin, 2009), pp. 1–74.
- [55] A. He, J. S. Lowengrub, and A. Belmonte, Modeling an elastic fingering instability in a reactive Hele-Shaw flow, *SIAM Appl. Math.* **72**, 842 (2012).
- [56] G. D. Carvalho, H. Gadêlha, and J. A. Miranda, Interfacial elastic fingering in a Hele-Shaw cell: A weakly nonlinear study, *Phys. Rev. E* **88**, 053006 (2013).
- [57] M. Zhao, A. Belmonte, S. Li, X. Li, and J. S. Lowengrub, Nonlinear simulations of elastic fingering in a Hele-Shaw cell, *J. Comput. Appl. Math.* **307**, 394 (2016).
- [58] A. Cebers and I. Javaitis, Dynamics of a flexible magnetic chain in a rotating magnetic field, *Phys. Rev. E* **69**, 021404 (2004).

- [59] M. Roper, R. Dreyfus, J. Baudry, M. Fermigier, and H. Stone, On the dynamics of magnetically driven elastic filaments, *J. Fluid Mech.* **554**, 167 (2006).
- [60] L. Carrillo, F. X. Magdaleno, J. Casademunt, and J. Ortín, Experiments in a rotating Hele-Shaw cell, *Phys. Rev. E* **54**, 6260 (1996).
- [61] E. Alvarez-Lacalle, J. Ortín, and J. Casademunt, Low viscosity contrast fingering in a rotating Hele-Shaw cell, *Phys. Fluids* **16**, 908 (2004).
- [62] E. Bayart, S. Deboeuf, F. Corson, A. Boudaoud, and M. Adda-Bedia, Measuring order in the isotropic packing of elastic rods, *Europhys. Lett.* **95**, 34002 (2011).
- [63] E. Bayart, A. Boudaoud, and M. Adda-Bedia, Tuning the ordered states of folded rods by isotropic confinement, *Phys. Rev. E* **89**, 012407 (2014).
- [64] G. D. Carvalho, H. Gadêlha, and J. A. Miranda, Stationary patterns in centrifugally driven interfacial elastic fingering, *Phys. Rev. E* **90**, 063009 (2014).
- [65] S. H. Strogatz, *Nonlinear Dynamics and Chaos: With Applications to Physics, Biology, Chemistry, and Engineering* (Addison-Wesley, New York, 1994).
- [66] V. M. Vassilev, P. A. Djondjorov, and I. M. Mladenov, Cylindrical equilibrium shapes of fluid membranes, *J. Phys. A: Math. Theor.* **41**, 435201 (2008).
- [67] S. K. Veerapaneni, R. Raj, G. Biros, and P. K. Purohit, Analytical and numerical solutions for shapes of quiescent two-dimensional vesicles, *Int. J. Nonlin. Mech.* **44**, 257 (2009).
- [68] L. Giomi, Softly constrained films, *Soft Matter* **9**, 8121 (2013).
- [69] J. E. Rim, P. K. Purohit, and W. S. Klug, Mechanical collapse of confined fluid membrane vesicles, *Biomech. Model. Mech.* **13**, 1277 (2014).
- [70] G. Napoli and A. Goriely, A tale of two nested elastic rings, *Proc. R. Soc. A* **473**, 20170340 (2017).
- [71] C. C. Donato, M. A. F. Gomes, and R. E. de Souza, Scaling properties in the packing of crumpled wires, *Phys. Rev. E* **67**, 026110 (2003).
- [72] Y. C. Lin, Y. W. Lin, and T. M. Hong, Crumpling wires in two dimensions, *Phys. Rev. E* **78**, 067101 (2008).
- [73] E. Pauné, M. Siegel, and J. Casademunt, Effects of small surface tension in Hele-Shaw multifinger dynamics: An analytical and numerical study, *Phys. Rev. E* **66**, 046205 (2002).
- [74] J. A. Miranda and E. Alvarez-Lacalle, Viscosity contrast effects on fingering formation in rotating Hele-Shaw flows, *Phys. Rev. E* **72**, 026306 (2005).
- [75] S. Genç and P. P. Phulé, Rheological properties of magnetorheological fluids, *Smart Mater. Struct.* **11**, 140 (2002).